



CHORUS

This is the accepted manuscript made available via CHORUS. The article has been published as:

Microscopic Theory of Resonant Soft-X-Ray Scattering in Materials with Charge Order: The Example of Charge Stripes in High-Temperature Cuprate Superconductors

David Benjamin, Dmitry Abanin, Peter Abbamonte, and Eugene Demler

Phys. Rev. Lett. **110**, 137002 — Published 26 March 2013

DOI: [10.1103/PhysRevLett.110.137002](https://doi.org/10.1103/PhysRevLett.110.137002)

Microscopic theory of resonant soft x-ray scattering in systems with charge order

David Benjamin,¹ Dmitry Abanin,¹ Peter Abbamonte,² and Eugene Demler¹

¹*Physics Department, Harvard University, Cambridge, Massachusetts 02138, USA*

²*Department of Physics and Frederick Seitz Materials Research Laboratory, University of Illinois, Urbana, IL 61801, USA*

(Dated: February 21, 2013)

We present a microscopic theory of resonant soft x-ray scattering (RSXS) that accounts for the delocalized character of valence electrons. Unlike past approaches based on local form factors, our functional determinant method treats realistic band structures. This method builds upon earlier theoretical work in mesoscopic physics and accounts for excitonic effects as well as the orthogonality catastrophe arising from interaction between the core hole and the valence band electrons. We show that the two-peak structure observed near the O K edge of stripe-ordered $\text{La}_{1.875}\text{Ba}_{0.125}\text{CuO}_4$ is due to dynamical nesting within the canonical cuprate band structure. Our results provide evidence for reasonably well-defined, high-energy quasiparticles in cuprates, and establishes RSXS as a bulk-sensitive probe of the electron quasiparticles.

PACS numbers: 78.70.Ck, 61.05.cp, 74.72.Gh, 71.45.Lr

Introduction.— Resonant soft x-ray scattering (RSXS) is a powerful technique for exploring strongly-correlated quantum materials [1–3]. While neutron and non-resonant x-ray scattering cross sections are dominated by the contributions of nuclei and core electrons, RSXS couples selectively to valence electrons and provides an enormously enhanced sensitivity [4] to many-body correlations [1–3, 5–15]. RSXS is able to study a wide class of materials, including those available only in small samples and those with buried interfaces [13, 14]. RSXS has recently been used to observe orbital order in manganites [2, 5, 6] and ruthenates [8], hole crystallization in spin ladders [7], and charge order in cuprates [3, 10, 15], nickelates [9], and manganites [11, 12].

Although qualitative interpretation of RSXS data has already yielded insights into a variety of strongly correlated materials, a complete quantitative understanding of these experiments is still lacking. Most analyses have adapted the use of atomic form factors from x-ray crystallography [1, 3, 10, 11]. The form factor concept assumes optical locality, which is valid for ordinary x-ray diffraction, but breaks down in the resonant case if valence states are delocalized. Some authors have attempted to account for nonlocality by defining cluster, rather than single-atom, form factors [5, 9]. But even this approach breaks down if valence states are propagating quasiparticles. Recently Abbamonte et al. [16] showed that neglecting the finite lifetime of core holes and interaction of valence electrons with core holes allows one to relate RSXS spectra to the local electron Green’s function measured in STM. However, these neglected effects are expected to play an important role and it is not clear how well this simplified analysis explains RSXS spectra in real materials. The state of affairs in RSXS should be contrasted to ARPES [17, 18] and STM [19–23], where one can often read off spectral functions directly from measurements, facilitating the comparison of theoretical models with experimental results.

In this paper we present the first microscopic model of elastic RSXS in systems with charge order in the valence band, such as striped high- T_c cuprates [20, 24–29]. Our method allows us to analyze RSXS spectra for itinerant valence electrons with realistic bandstructures. It accounts for excitonic effects and the orthogonality catastrophe arising from the interaction of valence electrons with core holes (for noninteracting valence electrons our analysis is exact) as well as the finite lifetime of core holes. We explain the two-peak spectrum observed in experiments at the O K edge of $\text{La}_{1.875}\text{Ba}_{0.125}\text{CuO}_4$ [3, 10] in terms of dynamical nesting of the “standard” cuprate band structure (see Figs. 1 and 2). We find that interaction of valence electrons with the core hole changes the spectrum significantly. We obtain quantitative agreement with the experimental data on underdoped $\text{La}_{1.875}\text{Ba}_{0.125}\text{CuO}_4$ (LBCO) and $\text{La}_{1.8-x}\text{Eu}_{0.2}\text{Sr}_x\text{CuO}_4$ (LESCO) [3, 10]. Our results directly connect RSXS at the O K edge to band structure, establishing it as a bulk-sensitive probe of electron quasiparticles complementary to ARPES and STM.

Theoretical formalism for elastic RSXS.— Following Ref. [16] we consider an effective single band model describing resonant absorption and emission of photons

$$\mathcal{H}_{\text{int}} = \sum_{j,\mathbf{k},\lambda} V(\mathbf{k}, \lambda) \left(d_j^\dagger c_j a_{\mathbf{k},\lambda} e^{i\mathbf{k}\cdot\mathbf{r}} + \text{h.c.} \right) \quad (1)$$

Here c_j and d_j annihilate electrons on site j in the core orbital and valence band respectively, $a_{\mathbf{k},\lambda}$ annihilates a photon with momentum \mathbf{k} and polarization $\hat{\epsilon}_{\mathbf{k},\lambda}$, and $V(\mathbf{k}, \lambda)$ are matrix elements whose precise form is unimportant. Resonant scattering is a second order process

$$I(\omega) = \sum_f \left| \sum_n \frac{\langle f | \mathcal{H}_{\text{int}} | n \rangle \langle n | \mathcal{H}_{\text{int}} | i \rangle}{E_i^N - \bar{E}_n^{N+1} + \omega + i\Gamma/2} \right|^2 \quad (2)$$

Here $|i\rangle$ is the initial state of the system with N electrons in the valence band and incoming photon \mathbf{k}_i ; $|n\rangle$ is the

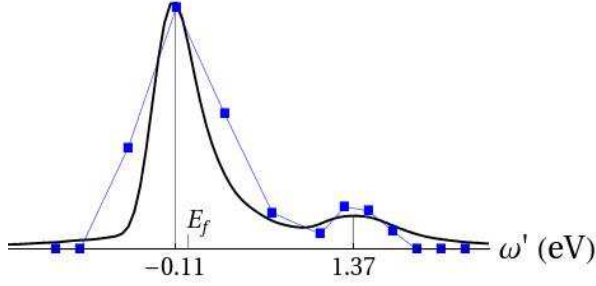


FIG. 1. Calculated RSEX spectrum for the canonical cuprate band-structure with period-4 charge order and core hole potential $U_0 = -250$ meV. The zero of $\omega' \equiv \omega + \xi_c - E_f$, where ξ_c is the core level energy, is the energy required to excite a core level to E_f in the absence of a core hole potential. Squares are LBCO data from Ref. [3]. The position of the first peak is determined by dynamical nesting and the core hole potential and is not related to E_f [36].

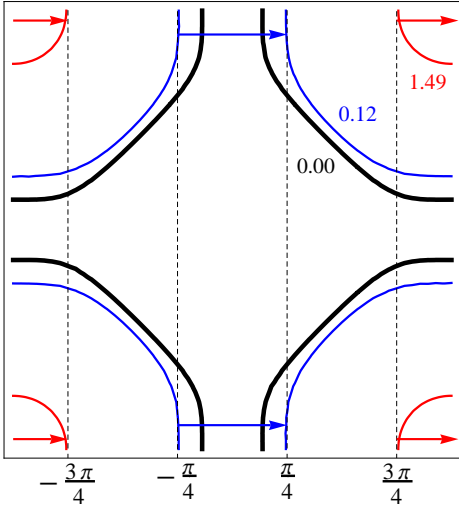


FIG. 2. Dynamical nesting in the cuprate band structure. Nested contours $E = E_f + 0.12$ eV and $E = E_f + 1.49$ are blue and red; the Fermi surface is black. The lines $k_x = -3\pi/4, -\pi/4, \pi/4, 3\pi/4$ (dashed) are a visual guide.

transient state with a core hole, $N + 1$ valence electrons, and no photons; $|f\rangle$ is the final state with no core hole, N valence electrons, and one outgoing photon with momentum \mathbf{k}_f . The transient state energy \tilde{E}_n^{N+1} includes the core hole potential. Γ is the decay rate of the core hole. We focus on elastic scattering, where $|f\rangle = |i\rangle$ and $\mathbf{Q} = \mathbf{k}_f - \mathbf{k}_i$ is an ordering wavevector.

Because the core hole is immobile it is created and refilled on the same site j and contributes the trivial matrix element $\langle 1|c_j^\dagger|0\rangle\langle 0|c_j|1\rangle = 1$. It may be subsumed into a static potential $U(\mathbf{r} - \mathbf{r}_j)$ that acts on the valence elec-

trons of the transient state. Therefore, Eq. (2) becomes

$$I(\omega, \mathbf{Q}) \propto \left| \sum_{j,n,\sigma} e^{-i\mathbf{Q}\cdot\mathbf{r}_j} \frac{\langle i|d_{j\sigma}|n\rangle\langle n|d_{j\sigma}^\dagger|i\rangle}{E_i - \tilde{E}_n^{N+1} + \omega + i\Gamma/2} \right|^2 \quad (3)$$

$$= \left| \sum_{j\sigma} e^{-i\mathbf{Q}\cdot\mathbf{r}_j} \int_0^\infty e^{-(i\omega+\Gamma)t} S_{j\sigma}(t) dt \right|^2, \quad (4)$$

where $S_{j\sigma}(t) = \langle i|d_{j\sigma}e^{-i\mathcal{H}_1(j)t}d_{j\sigma}^\dagger e^{i\mathcal{H}_0 t}|i\rangle$, $\mathcal{H}_{0(1)}$ is the Hamiltonian of the valence electrons with(out) the core hole potential, and matrix elements refer to the valence electron Fock space. Without a core hole potential, $\mathcal{H}_1 = \mathcal{H}_0$ and $S_{j\sigma}(t)$ reduces essentially to a retarded Green's function [16]. Eq. (4) applies to a thermal ensemble at temperature $T = 1/\beta$, provided that we use

$$S_{j\sigma}(t) = \frac{\text{Tr} \left[d_{j\sigma} e^{-i\mathcal{H}_1(j)t} d_{j\sigma}^\dagger e^{i\mathcal{H}_0 t} e^{-\beta\mathcal{H}_0} \right]}{\text{Tr} \left[e^{-\beta\mathcal{H}_0} \right]}. \quad (5)$$

Eqs. (4 - 5) apply to an arbitrary interacting valence band Hamiltonian and are generalized to multiple bands by adding orbital indices to electron operators and to matrix elements for absorption and emission. Below, we will limit our discussion to the model of non-interacting electrons. This assumption is justified as long as the lifetime of electron states in the valence band is longer than the core hole lifetime Γ^{-1} (see discussion below).

In the absence of pairing interactions the operators that define $S_{j\sigma}(t)$ break up into commuting spin- σ and spin- $\bar{\sigma}$ parts and the initial electron state is a direct product $|i_\sigma\rangle|i_{\bar{\sigma}}\rangle$. Hence $S_{j\sigma}(t) = S_j^{OC}(t)S_j^{FES}(t)$, where $S_j^{OC}(t) = \langle i_\sigma|e^{-i\mathcal{H}_1(j)t}e^{i\mathcal{H}_0 t}|i_\sigma\rangle$ and $S_j^{FES}(t) = \langle i_{\bar{\sigma}}|d_j e^{-i\mathcal{H}_1(j)t}d_j^\dagger e^{i\mathcal{H}_0 t}|i_{\bar{\sigma}}\rangle$. At non-zero temperature

$$S_j^{OC}(t) = \frac{\text{Tr} \left[e^{-i\mathcal{H}_1(j)t} e^{i\mathcal{H}_0 t} e^{-\beta\mathcal{H}_0} \right]}{\text{Tr} \left[e^{-\beta\mathcal{H}_0} \right]} \quad (6)$$

$$S_j^{FES}(t) = \frac{\text{Tr} \left[d_j e^{-i\mathcal{H}_1(j)t} d_j^\dagger e^{i\mathcal{H}_0 t} e^{-\beta\mathcal{H}_0} \right]}{\text{Tr} \left[e^{-\beta\mathcal{H}_0} \right]}, \quad (7)$$

where operators and traces refer to effective spinless systems polarized to $\bar{\sigma}$ and σ , respectively.

$S_j^{OC}(t)$ appears in the orthogonality catastrophe of x-ray absorption [30, 31]. It expresses the many-body overlap of the initial Fermi sea with the perturbed Fermi sea that time evolves under \mathcal{H}_1 . $S_j^{FES}(t)$ has been studied in the context of the Fermi edge singularity in resonant tunneling [32, 33], and in addition to the time evolution of the Fermi sea expresses the dynamics of an injected electron. A functional determinant method allows both to be expressed in terms of the *single-particle* matrices

$$\hat{H}_{0,1} : \mathcal{H}_{0,1} = (\hat{H}_{0,1})_{ij} d_i^\dagger d_j \text{ [31, 32, 34, 35]}$$

$$S_j^{OC}(t) = \det \left((1 - \hat{N}) + \hat{U}_j(t) \hat{N} \right) \quad (8)$$

$$S_j^{FES}(t) = S_j^{OC}(t) \left(\frac{\hat{N}}{1 - \hat{N}} + \hat{U}_j^{-1}(t) \right)_{jj}^{-1}, \quad (9)$$

where $\hat{N} \equiv (1 + \exp(\beta \hat{H}_0))^{-1}$ is the occupation number operator and $\hat{U}_j(t) \equiv e^{-i\hat{H}_1(j)t} e^{i\hat{H}_0 t}$ is the intermediate state time evolution operator. Standard steps [32, 34] work as follows: In a basis that diagonalizes \mathcal{H}_0 , $\mathcal{H}_0 = \sum_\alpha \xi_\alpha \hat{n}_\alpha$, the trace $\text{Tr} [e^{-\beta \mathcal{H}_0}]$ factors as $\prod_\alpha \sum_{n_\alpha=0,1} e^{-\beta n_\alpha \xi_\alpha} = \prod_\alpha (1 + e^{-\beta \xi_\alpha})$, which is the product of eigenvalues, hence the determinant, of $1 + e^{-\beta \mathcal{H}_0}$. By the Baker-Campbell-Hausdorff Lemma $e^{-i\mathcal{H}_1 t} e^{i\mathcal{H}_0 t} e^{-\beta \mathcal{H}_0} = e^W$, where W is quadratic, and hence $\text{Tr} [e^{-i\mathcal{H}_1(j)t} e^{i\mathcal{H}_0 t} e^{-\beta \mathcal{H}_0}] = \det (1 + e^{-i\mathcal{H}_1(j)t} e^{i\mathcal{H}_0 t} e^{-\beta \mathcal{H}_0})$. $S_j^{FES}(t)$ requires additional algebra [32] of the inserted d_j^\dagger and d_j [36].

We interpret Eq. (8) as follows: The determinant is a device for calculating overlaps of Slater determinant states, and its argument says to compute the overlap of $\langle i | e^{-i\mathcal{H}_1 t}$ and $e^{i\mathcal{H}_0 t} | i \rangle$. The operator \hat{N} determines which states are occupied in $|i\rangle$, while $1 - \hat{N}$ contributes a trivial factor of unity for unoccupied states. The additional matrix element in Eq. (9) corresponds to single-particle dynamics of the injected electron. It is a local Green's function for propagation of a single electron from site j to site j , modified by the Pauli-blocking term $N/(1 - N)$. For period- p order, one needs to sum over p inequivalent sites j . The determinant can be evaluated efficiently for a finite system, converging by a system size of 25×25 . Eqs. (4), (8), and (9) constitute a convenient formula for calculating RSXS spectra in the approximation of non-interacting electrons. They treat exactly the interaction of electrons with the core hole and finite lifetime of the core hole.

RSXS of cuprates.— We apply Eqs. (4) and (8-9) to charge order in an effective one-band model of the cuprates

$$H_0 = \sum_{\mathbf{k}} \xi_{\mathbf{k}} d_{\mathbf{k}}^\dagger d_{\mathbf{k}} + V \sum_{\mathbf{k}} \left(d_{\mathbf{k}+\mathbf{Q}}^\dagger d_{\mathbf{k}} + d_{\mathbf{k}}^\dagger d_{\mathbf{k}+\mathbf{Q}} \right). \quad (10)$$

Eq. (10) is a phenomenological mean-field description of charge ordering [25, 27, 37–40] that applies regardless of its microscopic origin. Possible mechanisms include electron-electron interactions, in which case charge order is often called stripes [29, 41–44], and nesting of the Fermi surface and electron-phonon interactions [45, 46]. We use the dispersion $\xi_{\mathbf{k}} = -\sum_{\mathbf{r}} e^{i\mathbf{k}\cdot\mathbf{r}} t_{\mathbf{r}} - \mu$ and parameters $t_{(1,0)} = 340$, $t_{(1,1)} = -32$, $t_{(2,0)} = 25$, $t_{(2,1)} = 31$ meV characteristic of LBCO [47]. For simplicity we ignore k_z dispersion, which would at most smear energy peaks by an amount $t_z \lesssim 50$ meV [47]. Fig. 1 presents an RSXS spectrum for a contact potential $U(\mathbf{r} - \mathbf{r}_j) = U_0 \delta_{\mathbf{r},\mathbf{r}_j}$.

Yukawa potentials yield similar results [36]. We have chosen a realistic core hole lifetime $\Gamma = 250$ meV.

Two peak structure. Fig. 1 shows the calculated RSXS intensity versus photon energy. The two peak structure of the spectrum agrees well with experiments [3, 10]. A simple argument shows that the two peaks are a robust feature of the cuprate band structure. In the limit of zero core hole potential the only non-trivial time evolution in the transient state is that of the photo-excited electron subject to the scattering potential of Eq. (10). RSXS intensity comes from scattering $|\mathbf{k}\rangle \rightarrow |\mathbf{k} + \mathbf{Q}\rangle$, which occurs most readily when $\xi_{\mathbf{k}}$, $\xi_{\mathbf{k}+\mathbf{Q}}$ are nearly degenerate. Intensity at energy E comes from points on the surface of constant energy E that are separated by wavevector \mathbf{Q} [37]. Peaks occur when this contour has segments nested by wavevector \mathbf{Q} , which yields large density of states for scattering. Equivalently, in this limit the energy domain expression Eq. (3) reduces to

$$I(\omega, \mathbf{Q}) \propto \left| \sum_{j,\phi} e^{-i\mathbf{Q}\cdot\mathbf{R}_j} \frac{(1 - n_F(E_\phi)) |\langle \phi | j \rangle|^2}{E_i - E_\phi + \omega + i\Gamma/2} \right|^2. \quad (11)$$

Eigenstates $|\phi\rangle$ of H_0 contribute in proportion to the \mathbf{Q} -component of their Fourier-transformed density. In the presence of a CDW potential, this is due to hybridization of $|\mathbf{k}\rangle$ and $|\mathbf{k} + \mathbf{Q}\rangle$, which nesting again maximizes. Unlike Fermi surface nesting, this dynamical nesting is a generic consequence of symmetry. Consider the two-dimensional cuprate Brillouin zone and period-4 CDW wavevector $\mathbf{Q} = (\pi/2, 0)$. Any Bloch state $|\mathbf{k}\rangle$ on the lines $k_x = -\pi/4$ and $k_x = 3\pi/4$ is degenerate with $|\mathbf{k} + \mathbf{Q}\rangle$. Constant energy contours tangent to the line $k_x = -\pi/4$ ($-3\pi/4$) are also tangent to $k_x = \pi/4$ ($3\pi/4$); these symmetry-equivalent segments are dynamically nested. Fermi surface nesting requires the particular contour $E = E_f$ to be tangent to the lines. Dynamical nesting occurs when *some* energy contour is tangent to the lines (see Fig. 2). The energy contours of the chosen dispersion exhibiting dynamic nesting correspond to energies 0.1 eV and 1.5 eV above the Fermi level— which are separated by nearly the same amount as RSXS peaks.

Dynamical nesting explains the spectrum and its two peaks qualitatively but does not give the correct relative weights of the two peaks [36]. Including the core hole potential yields quantitative agreement with experiments. The core hole potential has a weak effect on the energy separation between the two peaks but dramatically suppresses the high-energy peak [36]. A core hole potential strength $U_0 = -250$ meV, which is reasonable for a screened core hole interacting with valence electrons, reproduces the experimental ratios of peak intensities. The discussion of Ref. [16] connecting the RSXS spectrum to the electron spectral function thus remains largely accurate in the presence of a weak core hole potential. However, strong core hole potentials yield spectra with qualitative features, such as a missing high-energy peak, that

would mislead analyses based only on the spectral function. For example, we attribute the absence of a second peak in RSXS at the Cu $L_{3/2}$ edge [3] to a strong Cu core hole potential. The spectrum is robust to changes in the core hole lifetime Γ , which broadens the peaks, and the CDW strength V , which scales the overall intensity. Small changes in the band structure have little effect.

Our calculations provide the first quantitative explanation for the two peak structure observed in LBCO and LESCO [3, 10]. An earlier interpretation of the two peaks as arising from the lower and upper Hubbard bands, the so-called “spatially-modulated Mottness”, was not supported by quantitative analysis. Moreover, a separation of ~ 1.9 eV between peaks is found in x-ray absorption spectroscopy (XAS) of LBCO and LSCO [3, 48]. According to the lower/upper Hubbard band interpretation, in which between peaks there is a gap, the separation between peaks in RSXS must be at least as large as the separation in XAS. Thus we think that dynamical nesting is more natural interpretation of the two peak structure observed in LBCO and LESCO.

Discussion.— We now comment on the choice of band structure. Ab-initio LDA calculations on LSCO give $t_{(1,0)} = 430$, $t_{(1,1)} = -40$, $t_{(2,0)} = 30$, $t_{(2,1)} = 35$ meV [47] while fitting of the ARPES spectra gives $t_{(1,0)} = 250$, $t_{(1,1)} = -25$, $t_{(2,0)} = 20$, $t_{(2,1)} = 28$ [47]. The ratios among tight-binding parameters are nearly identical for both cases, so the band structure is well-known up to an overall scaling factor. Two peaks appear in the RSXS spectra for both band structures with nearly the same relative intensities. We find that taking either the LDA or ARPES dispersions gives peaks separated by 1.7 and 1.3 eV. We obtain the best fit to RSXS data by choosing parameters halfway between the two. It is not surprising that band structure obtained from the ARPES data does not provide the best agreement with the RSXS spectra. ARPES data only exist within 200 meV of the Fermi surface [49], where the renormalization effect due to interactions is strongest, while we are interested in features at much higher energy. Additionally, it has been suggested that ARPES tends to underestimate electron dispersion relative to x-ray experiments [47, 50]. Another important issue is our approximation of non-interacting electrons. The key quantity of our analysis is a generalized propagator (5). Interactions cause electrons to decay into other excitations, but as far as the Green’s function is concerned this simply contributes an imaginary part to the electron’s self-energy (the effective one-band model already incorporates renormalization via the *real* part of self-energies). If the electron decays slowly compared to the core hole any broadening introduced by electron interactions will be hidden within the width Γ . Conversely, rapid electron decay would broaden peaks into oblivion. Therefore, the presence of peaks in an RSXS spectrum puts an upper bound on the imaginary self-energy and implies that excitations resemble well-

defined quasiparticles. Recent DMFT calculations [51] have found long-lived electron quasiparticles in the Hubbard model well above the Fermi energy, in contrast to short-lived hole-like excitations. RSXS, which probes high-energy electron excitations, complements ARPES, which probes hole-like excitations, and quantum oscillation experiments [52, 53], which probe excitations near the Fermi energy.

Outlook.—The predictions of our model can be checked in future experiments. For example, recent work on charge order in underdoped YBCO [15], which was performed at energies corresponding to Cu L edges, could be repeated at the O K edge. We expect, as in LBCO, two peaks at energies determined by band structure. Also, systems with checkerboard charge order, with coexisting Fourier components \mathbf{Q}_x and \mathbf{Q}_y , will exhibit a harmonic at $\mathbf{Q}_x + \mathbf{Q}_y$. If the latter harmonic is sufficiently strong, an RSXS signal will appear at this wavevector. One can see that this ordering wavevector also has dynamical nesting at two energies, so we expect to find a two peak spectrum[54].

Summary.— We have developed a microscopic model of RSXS that takes into account the itinerant character of valence electrons and excitonic effects. We showed that a simple physical picture of dynamical nesting found in the canonical band structure of cuprates gives rise to a two peak structure, while the core hole potential is necessary for quantitative agreement with the data. Our analysis shows that even at high energies electronic excitations behave like sufficiently well-defined quasiparticles described by the canonical band structure.

Acknowledgements.— We thank A. Georges and J. Sau for useful discussions. This work was supported by Harvard-MIT CUA, NSF Grant No. DMR-07-05472, and the ARO-MURI on Atomtronics (DB, DA, ED); and the U.S. Department of Energy grant DE-FG02-06ER46285 (PA).

-
- [1] P. Abbamonte, L. Venema, A. Rusydi, G. A. Sawatzky, G. Logvenov, and I. Bozovic, *Science (New York, N.Y.)* **297**, 581 (2002).
- [2] S.B. Wilkins, P.D. Spencer, P.D. Hatton, S.P. Collins, M.D. Roper, D. Prabhakaran, and A.T. Boothroyd, *Physical Review Letters* **91**, 167205 (2003).
- [3] P. Abbamonte, A. Rusydi, S. Smadici, G. D. Gu, G. A. Sawatzky, and D. L. Feng, *Nature Physics* **1**, 155 (2005).
- [4] For example, in the case of the oxygen K edge in LBCO and LSCO the cross section for charge carriers is four orders of magnitude greater at resonance than away from resonance [14].
- [5] S.S. Dhesi, A. Mirone, C. De Nadaï, P. Ohresser, P. Bencok, N.B. Brookes, P. Reutler, A. Revcolevschi, A. Tagliiferri, O. Toulemonde, and G. van der Laan, *Physical Review Letters* **92**, 056403 (2004).
- [6] S. Grenier, J. Hill, D. Gibbs, K. Thomas, M. Zimmermann, C. Nelson, V. Kiryukhin, Y. Tokura, Y. Tomioka, D. Casa, T. Gog, and C. Venkataraman, *Physical Review B* **69**, 134419 (2004).
- [7] P. Abbamonte, G. Blumberg, A. Rusydi, A. Gozar, P. G. Evans, T. Siegrist, L. Venema, H. Eisaki, E. D. Isaacs, and G. A. Sawatzky, *Nature* **431**, 1078 (2004).
- [8] I. Zegkinoglou, J. Strempler, C.S. Nelson, J.P. Hill, J. Chakhalian, C. Bernhard, J.C. Lang, G. Srajer, H. Fukazawa, S. Nakatsuji, Y. Maeno, and B. Keimer, *Physical Review Letters* **95**, 136401 (2005).
- [9] C. Schüßler-Langeheine, J. Schlappa, A. Tanaka, Z. Hu, C.F. Chang, E. Schierle, M. Benomar, H. Ott, E. Weschke, G. Kaindl, O. Friedt, G.A. Sawatzky, H.-J. Lin, C.T. Chen, M. Braden, and L.H. Tjeng, *Physical Review Letters* **95**, 156402 (2005).
- [10] J. Fink, E. Schierle, E. Weschke, J. Geck, D. Hawthorn, V. Soltwisch, H. Wadati, H.-H. Wu, H.A. Dürr, N. Wizent, B. Büchner, and G.A. Sawatzky, *Physical Review B* **79**, 100502 (2009).
- [11] J. Herrero-Martín, J. García, G. Subías, J. Blasco, M.C. Sánchez, and S. Stanescu, *Physical Review B* **73**, 224407 (2006).
- [12] E. Nazarenko, J. E. Lorenzo, Y. Joly, J. L. Hodeau, D. Mannix, and C. Marin, *Physical Review Letters* **97**, 056403 (2006).
- [13] S. Smadici, P. Abbamonte, A. Bhattacharya, X. Zhai, B. Jiang, A. Rusydi, J.N. Eckstein, S.D. Bader, and J.-M. Zuo, *Physical Review Letters* **99**, 196404 (2007).
- [14] S. Smadici, J.C.T. Lee, S. Wang, P. Abbamonte, G. Logvenov, A. Gozar, C. DevilleCavellin, and I. Bozovic, *Physical Review Letters* **102**, 107004 (2009).
- [15] G. Ghiringhelli, M. L. Tacon, M. Minola, S. Blanco-Canosa, C. Mazzoli, N. B. Brookes, G. M. De Luca, A. Frano, D. G. Hawthorn, F. He, T. Loew, M. M. Sala, D. C. Peets, M. Salluzzo, E. Schierle, R. Sutarto, G. A. Sawatzky, E. Weschke, B. Keimer, and L. Braicovich, (2012), arXiv:1207.0915.
- [16] P. Abbamonte, E. Demler, J. C. S. Davis, and J.-C. Campuzano, (2011), arXiv:1112.5112.
- [17] A. Damascelli and Z.-X. Shen, *Reviews of Modern Physics* **75**, 473 (2003).
- [18] D. Lu, I. M. Vishik, M. Yi, Y. Chen, R. G. Moore, and Z.-X. Shen, *Annual Review of Condensed Matter Physics* **3**, 129 (2012).
- [19] O. Fischer, M. Kugler, I. Maggio-Aprile, C. Berthod, and C. Renner, *Reviews of Modern Physics* **79**, 353 (2007).
- [20] J. E. Hoffman, E. W. Hudson, K. M. Lang, V. Madhavan, H. Eisaki, S. Uchida, and J. C. Davis, *Science (New York, N.Y.)* **295**, 466 (2002).
- [21] K. McElroy, D.-H. Lee, J. E. Hoffman, K. M. Lang, J. Lee, E. W. Hudson, H. Eisaki, S. Uchida, and J. C. Davis, *Phys. Rev. Lett.* **94**, 197005 (2005).
- [22] M. Vershinin, S. Misra, S. Ono, Y. Abe, Y. Ando, and A. Yazdani, *Science* **303**, 1995 (2004).
- [23] C. Howald, H. Eisaki, N. Kaneko, M. Greven, and A. Kapitulnik, *Physical Review B* **67**, 014533 (2003).
- [24] J. M. Tranquada, B. J. Sternlieb, J. D. Axe, Y. Nakamura, and S. Uchida, *Nature* **375**, 561 (1995).
- [25] S. A. Kivelson, I. P. Bindloss, V. Oganesyan, J. M. Tranquada, A. Kapitulnik, and C. Howald, *Reviews of Modern Physics* **75**, 1201 (2003).
- [26] A.J. Millis and M.R. Norman, *Physical Review B* **76**, 220503 (2007).
- [27] M. Vojta, *Advances in Physics* **58**, 699 (2009).
- [28] E. Berg, E. Fradkin, S. A. Kivelson, and J. M. Tranquada, *New Journal of Physics* **11**, 115004 (2009).
- [29] J. Zaanen and O. Gunnarsson, *Physical Review B* **40**, 7391 (1989).
- [30] P. Nozières and C. de Dominicis, *Physical Review* **178**, 1097 (1969).
- [31] M. Combescot and P. Nozières, *Journal de Physique* **32**, 913 (1971).
- [32] D.A. Abanin and L.S. Levitov, *Physical Review Letters* **93**, 126802 (2004).
- [33] D.A. Abanin and L.S. Levitov, *Physical Review Letters* **94**, 186803 (2005).
- [34] I. Klich, in *Quantum Noise in Mesoscopic Physics*, edited by Y. Nazarov (Springer, 2003).
- [35] B.A. Muzykantskii and Y. Adamov, *Physical Review B* **68**, 155304 (2003).
- [36] See Supplemental Material for detailed derivation of trace formulae and variation of core hole potential and band structure.
- [37] D. Podolsky, E. Demler, K. Damle, and B.I. Halperin, *Physical Review B* **67**, 094514 (2003).
- [38] A. Hackl, M. Vojta, and S. Sachdev, *Physical Review B* **81**, 045102 (2010).
- [39] H. Yao, D.-H. Lee, and S. Kivelson, *Physical Review B* **84**, 012507 (2011).
- [40] I. Martin, G. Ortiz, A. V. Balatsky, and A. R. Bishop, *International Journal of Modern Physics B* **14**, 3567 (2000).
- [41] K. Machida, *Physica C: Superconductivity* **158**, 192 (1989).
- [42] M. Kato, K. Machida, H. Nakanishi, and M. Fujita, *Journal of the Physics Society Japan* **59**, 1047 (1990).
- [43] H.J. Schulz, *Physical Review Letters* **64**, 1445 (1990).
- [44] O. Andersen, A. Liechtenstein, O. Rodriguez, I. Mazin, O. Jepsen, V. Antropov, O. Gunnarsson, and S. Gopalan, *Physica C: Superconductivity* **185-189**, 147 (1991).
- [45] J.-X. Li, C.-Q. Wu, and D.-H. Lee, *Physical Review B* **74**, 184515 (2006).
- [46] K. M. Shen, F. Ronning, D. H. Lu, F. Baumberger, N. J. C. Ingle, W. S. Lee, W. Meevasana, Y. Kohsaka, M. Azuma, M. Takano, H. Takagi, and Z.-X. Shen, *Science (New York, N.Y.)* **307**, 901 (2005).
- [47] R. S. Markiewicz, S. Sahrakorpi, M. Lindroos, H. Lin, and A. Bansil, *Physical Review B* **72**, 054519 (2005).

- [48] D. C. Peets, D. G. Hawthorn, K. M. Shen, Y.-J. Kim, D. S. Ellis, H. Zhang, S. Komiya, Y. Ando, G. A. Sawatzky, R. Liang, D. A. Bonn, and W. N. Hardy, *Physical Review Letters* **103**, 087402 (2009).
- [49] A. Ino, C. Kim, M. Nakamura, T. Yoshida, T. Mizokawa, A. Fujimori, Z.-X. Shen, T. Kakeshita, H. Eisaki, and S. Uchida, *Physical Review B* **65**, 094504 (2002).
- [50] S. Hüfner, *Photoelectron Spectroscopy: Principles and Applications* (Springer, 2003) p. Table 4.5.
- [51] A. Georges, unpublished.
- [52] N. Doiron-Leyraud, C. Proust, D. LeBoeuf, J. Levallois, J.-B. Bonnemaison, R. Liang, D. A. Bonn, W. N. Hardy, and L. Taillefer, *Nature* **447**, 565 (2007).
- [53] B. Vignolle, D. Vignolles, D. LeBoeuf, S. Lepault, B. Ramshaw, R. Liang, D. Bonn, W. Hardy, N. Doiron-Leyraud, A. Carrington, N. Hussey, L. Taillefer, and C. Proust, *Comptes Rendus Physique* **12**, 446 (2011).
- [54] D. Benjamin, unpublished.